The non-oscillatory reconstruction of the polynomials $R_j(x, t^n)$, which is the heart of the method, is based on our Central-WENO reconstruction outlined below. An *exact* evolution of w, based on integration of the conservation law over the staggered cell, $I_{j+1/2}$, then reads

$$\overline{w}_{j+1/2}^{n+1} = \frac{1}{\Delta x} \int\limits_{I_{j+1/2}} w(x, t^n) \, \mathrm{d}x - \frac{1}{\Delta x} \int\limits_{t^n}^{t^{n+1}} \left[f\left(w(x_{j+1}, \tau)\right) - f\left(w(x_j, \tau)\right) \right] \mathrm{d}\tau.$$

The first integral is the staggered cell-average at time t^n, $\overline{w}_{j+1/2}^n$, which can be computed directly from the above reconstruction. Due to the staggering, the time integrals of the flux are computed in smooth regions (up to a certain CFL condition) and hence, they can be approximated by any sufficiently accurate quadrature formula (e.g., for a fourth-order method one can use Simpson's rule),

$$\frac{1}{\Delta x} \int\limits_{\tau=t^n}^{t^{n+1}} \left[f\left(w(x_j, \tau)\right) \right] \mathrm{d}\tau \sim \lambda \sum_{l=0}^{m} \gamma_l \left[f\left(\widehat{w}(x_j, t^n + \beta_l \Delta t)\right) \right]. \tag{3}$$

Here, γ_l, are the quadrature weights and $t^n + \beta_l \Delta t$ are the intermediate levels. The intermediate values required in (3), $\widehat{w}(x_j, t^n + \beta_l \Delta t)$, are predicted using either a Taylor expansion or a Runge–Kutta (RK) method which is more efficient (in particular, for high-order methods and for systems). Our numerical scheme utilized a RK method with a natural continuous extension (taken from [12]) which requires only one step of the RK method from which the rest of the required values can be reconstructed with the desired accuracy (consult [6]).

2.2. The CWENO reconstruction

Below we outline the CWENO reconstruction and refer to [6] for more details. Our reconstruction is a modification of the reconstruction procedure suggested in [4,7]. There, in the so-called *Weighted Essentially Non-Oscillatory* (WENO) method, instead of selecting one stencil according to a non-oscillatory criterion, the interpolant is constructed by taking a convex combination of all candidate stencils. The weights of this combination are determined through a non-linear computation which is based on the local smoothness of the stencil. Every stencil is weighted according to the oscillations which it might create. In discontinuous regions, e.g., the weights will be biased towards the stencils in the smoother regions. Since, effectively, in smooth regions the linear combination of the different stencils can be interpreted as a wide stencil, a higher-order scheme can be constructed using polynomials of low degree.

We derive a fourth-order method which is based on a piecewise-parabolic reconstruction step. Our interpolant takes the form

$$R_j(x) = \sum_{k=j-1}^{j+1} w_k^j P_k(x), \qquad \sum_{k=j-1}^{j+1} w_k^j = 1, \quad w_k^j \geqslant 0, \tag{4}$$

where $P_k(x)$ are polynomials reconstructed using different stencils around x_j. For example, $P_{j-1}(x)$ is the polynomial based on the left stencil $\{x_{j-2}, x_{j-1}, x_j\}$. The reconstructed polynomial must satisfy *conservation* requirements,

$$\frac{1}{h} \int\limits_{I_k} R_j(x) \, \mathrm{d}x = \overline{u}_k, \quad k = j-1, j, j+1,$$

and *accuracy* requirements, imposing that the average of the reconstruction on the half cells, $I_j^- :=$ $[x_{j-1/2}, x_j]$, $I_j^+ := [x_j, x_{j+1/2}]$, must satisfy (with s denoting the degree of accuracy),

$$\frac{1}{2h} \int_{I_j^\pm} R_j(x, t^n) \, dx = \frac{1}{2h} \int_{I_j^\pm} u(x, t^n) \, dx + O(h^s).$$

For the point-values we require $R_j(x_j, t^n) = u(x_j, t^n) + O(h^s)$. In the predictor step, we use a separate reconstruction for the derivatives of the fluxes, $f'(u(x, t))$, for which we require $R'_f(x_j, t^n) = f'(u(x_j, t^n)) + O(h^{s-1})$. Non-oscillatory requirements (in the sense of ENO/WENO) enter through the choice of the weights w_k^j in (4).

Each polynomial, $P_k(x)$, can be written in the form

$$P_k(x) = \tilde{u}_k + \tilde{u}'_k(x - x_k) + \frac{1}{2}\tilde{u}''_k(x - x_k)^2, \quad k = j - 1, j, j + 1.$$

The reconstructed point-values, $\tilde{u}_k$, and the reconstructed discrete first and second derivatives, $\tilde{u}'_k, \tilde{u}''_k$, are uniquely determined by the interpolation requirements as ($k = j - 1, j, j + 1$)

$$\tilde{u}''_k = \frac{\overline{u}_{k+1} - 2\overline{u}_k + \overline{u}_{k-1}}{h^2}, \qquad \tilde{u}'_k = \frac{\overline{u}_{k+1} - \overline{u}_{k-1}}{2h}, \qquad \tilde{u}_k = \overline{u}_k - \frac{h^2}{24}\tilde{u}''_k.$$

Following the notations of [4], convexity is guaranteed when the weights, w_k^j, are written as (with $k = j - 1, j, j + 1$),

$$w_k^j = \frac{\alpha_k^j}{\alpha_{j-1}^j + \alpha_j^j + \alpha_{j+1}^j}, \qquad \alpha_k^j = \frac{C_k}{(\varepsilon + IS_k^j)^p}, \quad C_k \geqslant 0.$$

The constant ε appears in the denominator in order to prevent it from vanishing. In [4] an $\varepsilon = 10^{-6}$ was chosen empirically and we use the same ε. In [7] the value of p was taken as one plus the degree of the reconstruction polynomial, while in [4] a $p = 2$ was empirically selected and here we use the same. The constants C_k are chosen such as to gain maximum accuracy in smooth regions. The accuracy requirements for the central and upwind frameworks are different. This results with different weights for the CWENO reconstruction compared with those obtained in upwind WENO. We utilize two sets of constants, one for the computation of cell-averages on half-cells, and the other for the computation of the derivatives of the fluxes. These constants are displayed in Table 1.

Table 1
The constants, C_k, of the Central-WENO reconstruction

	C_{j-1}	C_j	C_{j+1}	Accuracy
Cell-averages	$\frac{3}{16}$	$\frac{5}{8}$	$\frac{3}{16}$	h^5
Derivatives	$\frac{1}{6}$	$\frac{2}{3}$	$\frac{1}{6}$	h^4
Point-values	any symmetric combination			h^4

Finally, there are several approaches to compute the smoothness indicators IS_k^j (consult [4,7]). We use the measure taken from [4], which sums the L^2-norms of the first and second derivatives, where $P_k^{(l)}$ denotes the lth derivative of $P_k(x)$,

$$IS_k^j = \sum_{l=1}^{2} \int_{x_{j-1/2}}^{x_{j+1/2}} h^{2l-1} \left(P_k^{(l)} \right)^2 \, \mathrm{d}x, \quad k = j-1, j, j+1.$$

3. Numerical examples

We present several numerical examples demonstrating the promising TV properties of the 1D CWENO *fourth-order* method. Our numerical results suggest that the CWENO method is TVB. Our first example is the linear advection problem, $u_t + u_x = 0$, subject to the initial data, $u_0(x) = \sin(\pi x)$, and to periodic boundary conditions on $[-1, 1]$. The integration time is $T = 1.5$. Following [6], the CFL was taken as $1.8/7$. Note that the TV of the exact solution equals 4, and remains constant along the evolution. Fig. 1 presents the TV of the CWENO approximate solution, which is computed using the point-values obtained with the CWENO reconstruction from the cell-averages.

The value of the TV of the approximate solution never increases above the exact TV. The amplitude of the oscillations decrease as the mesh is refined and it approaches the theoretical value. The TV of the numerical solution is different from that of the exact solution for two reasons: First, the TV is computed on a discrete set of points, and second, the discrete values of the numerical solution are not exact. The computation on a discrete set of points is responsible for both the oscillations and the modulation phenomena observed in Fig. 1. Same phenomena are observed if we sample the exact solution in a discrete set of points in space and time. The amplitude of the oscillation decreases roughly by a factor four when the grid points are doubled, indicating a second order effect. This is exactly what one would expect from computing the TV of the exact solution on a grid. The TV would be slightly less than 4, because the grid points will not be exactly on the extrema, but they will be displaced by a distance $O(h)$, and therefore the value of the function on those points will differ by an amount $O(h^2)$ from the extrema. Also, the slow variation on the amplitude of the oscillation is due to the fact that the TV is not computed for all times, but only for discrete times. If they were computed for all times, then the distance between two crests would be equal to the grid spacing h (divided by the propagation speed, which in this case is 1). The distance is larger, because the discrete solution is realized at discrete times. If $\Delta t = \Delta x/2$, then the oscillations would be of the same amplitude. When Δt differs slightly from $\Delta x/2$, then the usual modulation effect develops. Hence, the period of the modulation strongly depends on the Courant number.

Our next example is the Burgers equation, $u_t + (\frac{1}{2}u^2)_x = 0$, subject to the initial conditions, $u(x, t = 0) = 1 + 0.5 \sin(\pi x)$, and to periodic boundary conditions on $[-1, 1]$. Once again, the integration time is $T = 1.5$. The results are displayed in Fig. 2. Each frame contains two graphs: the dotted line corresponds to the TV of the exact solution, while the solid line corresponds to the TV of the approximate solution. A shock is created at time $T = 2/\pi$.

The TV of the approximate solution has the same behavior as the TV of the exact solution. Most importantly, again, it never increases above the theoretical value and it tends to the exact TV value when the mesh is refined. Even in the coarse grids the slope of the decrease after the shock is the same for both approximate and exact solution, though the starting time of that decrease is smaller for the approximate
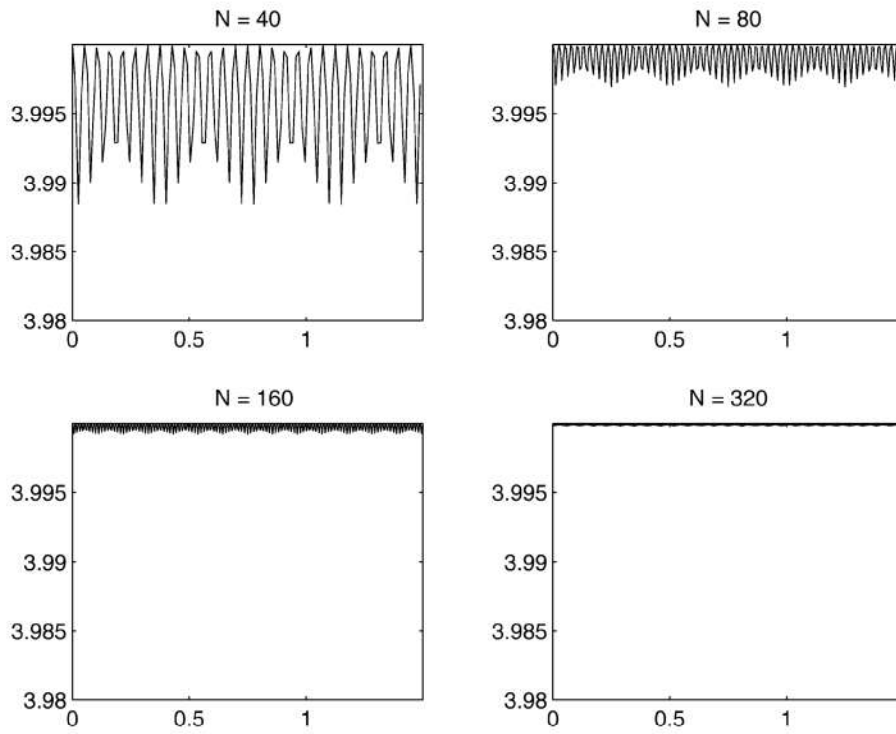
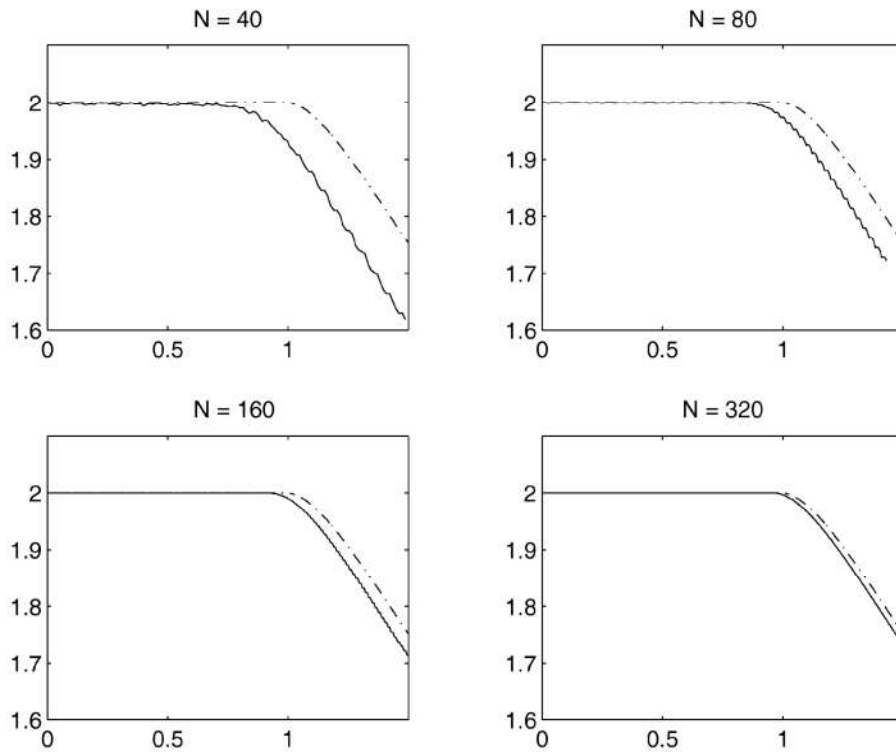Fig. 1. TV of the solution to a linear advection problem.

Fig. 2. TV of the solution to Burgers equation. Dotted line—TV computed from the exact solution. Solid line—TV computed from the CWENO approximated solution.
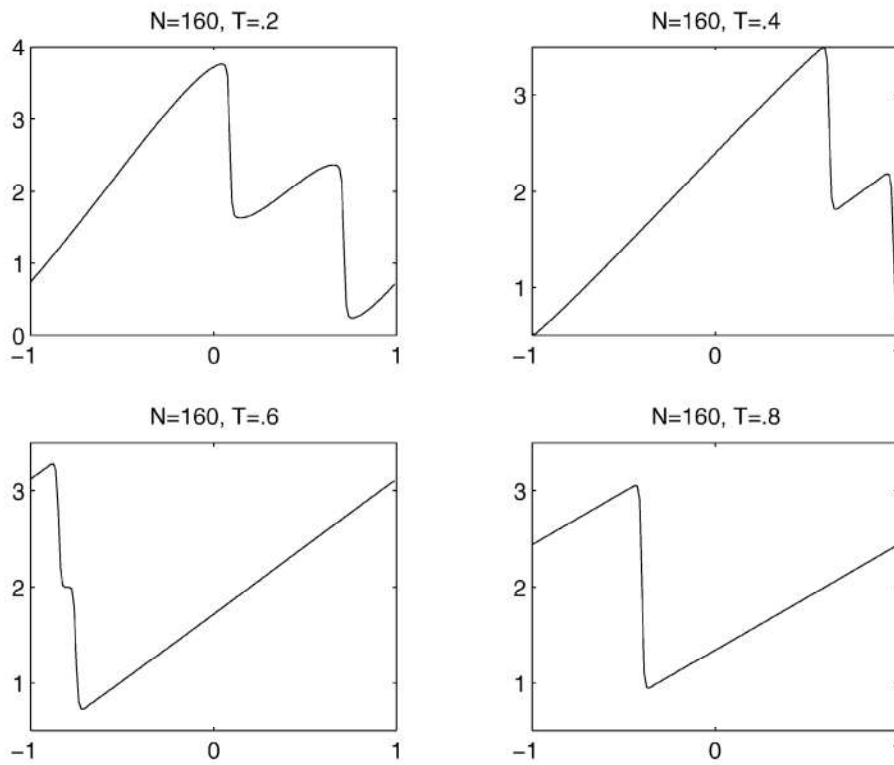
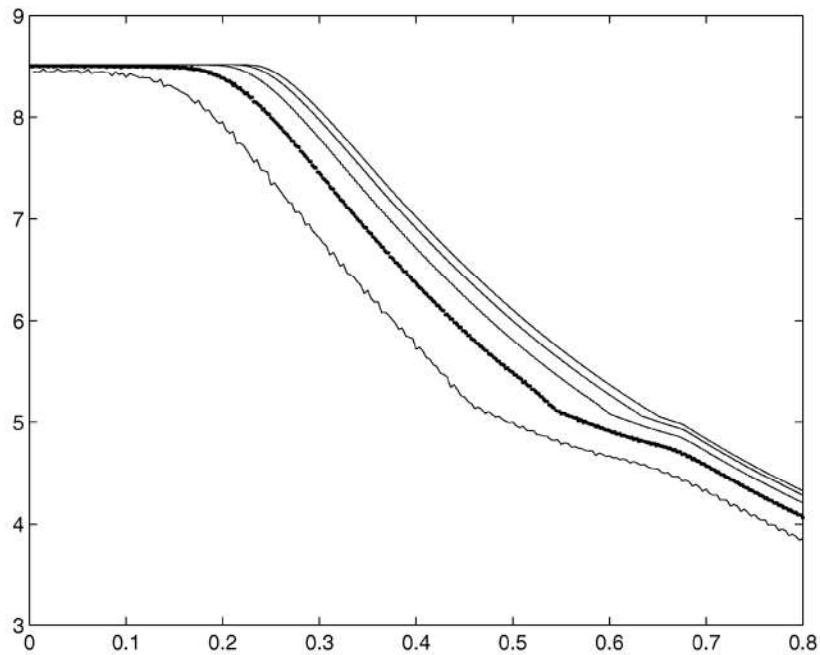Fig. 3. The solution of Burgers equation with two interacting shocks.

Fig. 4. TV of the solution to the Burgers equation with two interacting shocks. The curves correspond to $N = 40, 80, 160, 320, 640$, in an increasing order.

solution. The results are impressive even in the $N = 40$ plot, taking into account that the 1D CWENO reconstruction is based on a 5-point stencil. Finally, we would like to point the appearance of a stair-case behavior in all pictures, whose magnitude decreases as the mesh is refined, we conjecture that this stair-case behavior is due to the staggering–de-staggering mechanism.

Our last example is of two discontinuities interacting with each other. Once again we solve the periodic Burgers equation $u_t + (\frac{1}{2}u^2)_x = 0$, with the initial condition, $u_0 = 2 - \sin(\pi x) + \sin(2\pi x)$. This initial condition generates two discontinuities, one moving faster that the other, eventually combining into one discontinuity. We run the fourth-order CWENO method with $\lambda = 0.25 \cdot \frac{2}{7}$ (the maximum speed is 4 and the critical Courant number is $\frac{2}{7}$).

Fig. 3 presents the behavior of the solution in time. It is clear that two shocks form and that slightly after $T = 0.6$, they merge into one shock. Fig. 4 contains various plots of the total variation for different grids. The grids are $N = 40, 80, 160, 320, 640$, with the curve corresponding to $N = 40$ being the lower one.

Clearly, no undesirable behavior is detected when the two shocks merge. It looks as if the TVD is monotonically converging, along with the fluctuations which converge to zero. The delay in the beginning of the decrease in the TV is related to the decrease in the numerical diffusion as the grid is refined.

References

[1] F. Bianco, G. Puppo, G. Russo, High order central schemes for hyperbolic systems of conservation laws, SIAM J. Sci. Comput. 21 (1) (1999) 294–322.

[2] K.O. Friedrichs, P.D. Lax, Systems of conservation equations with a convex extension, Proc. Nat. Acad. Sci. 68 (1971) 1686–1688.

[3] A. Harten, B. Engquist, S. Osher, S. Chakravarthy, Uniformly high order accurate essentially non-oscillatory schemes III, J. Comput. Phys. 71 (1987) 231–303.

[4] G.-S. Jiang, C.-W. Shu, Efficient implementation of weighted ENO schemes, J. Comput. Phys. 126 (1996) 202–228.

[5] R.J. LeVeque, Numerical Methods for Conservation Laws, Lectures in Mathematics, Birkhäuser, Basel, 1992.

[6] D. Levy, G. Puppo, G. Russo, Central WENO schemes for hyperbolic systems of conservation laws, M2AN 33 (3) (1999) 547–571.

[7] X.-D. Liu, S. Osher, T. Chan, Weighted essentially non-oscillatory schemes, J. Comput. Phys. 115 (1994) 200–212.

[8] X.-D. Liu, E. Tadmor, Third order nonoscillatory central scheme for hyperbolic conservation laws, Numer. Math. 79 (1998) 397–425.

[9] H. Nessyahu, E. Tadmor, Non-oscillatory central differencing for hyperbolic conservation laws, J. Comput. Phys. 87 (2) (1990) 408–463.

[10] C.-W. Shu, Essentially non-oscillatory and weighted essentially non-oscillatory schemes for hyperbolic conservation laws, ICASE Report 97-65, 1997.

[11] E. Tadmor, Approximate solutions of nonlinear conservation laws, in: A. Quarteroni (Ed.), Advanced Numerical Approximation of Nonlinear Hyperbolic Equations, Lecture Notes in Mathematics, Springer, Berlin, 1998.

[12] M. Zennaro, Natural continuous extensions of Runge–Kutta methods, Math. Comp. 46 (1986) 119–133.